

Supplementary Information

Bioinspired Polydopamine Supported on Oxygen-Functionalized Carbon Cloth as a High-Performance 1.2 V Aqueous Symmetric Metal-Free Supercapacitor

Masumeh Moloudi^a, Mohammad S. Rahmanifar^b, Abolhassan Noori^a, Xueying Chang^c, Richard B. Kaner^{*,c}, and Mir F. Mousavi^{*,a}

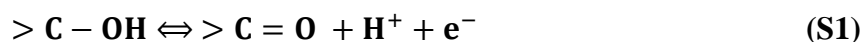
^a Department of Chemistry, Faculty of Basic Sciences, Tarbiat Modares University, Tehran, P.O. Box 14115-175, Iran, E-mail: mousavim@modares.ac.ir

^b Faculty of Basic Sciences, Shahed University, Tehran 3319118-651, Iran

^c Department of Chemistry and Biochemistry, Department of Materials Science and Engineering, and California NanoSystems Institute, University of California, Los Angeles (UCLA), CA 90095, USA, E-mail: kaner@chem.ucla.edu

1.1. Functionalization of Carbon Cloth

We used two methods for carbon cloth functionalization in order to study the role of the carbon cloth functionality on the capacitive performance of the electrode. In the first method, we performed an acid treatment for chemical functionalization of the carbon cloth with a 1:3 (v:v) mixture of concentrated HNO₃:H₂SO₄ at 60 °C for 2 h. As shown in **Figure S1a**, *via* the second functionalization method, carbon cloth pieces were treated with a KMnO₄ (1.0 mg) incorporated concentrated 1:2 (v:v) HNO₃:H₂SO₄ mixture at 35 °C for 1 h. **Figure S1b** shows CV curves of the pristine carbon cloth (CC) as well as carbon cloth functionalized via a mixed acidic solution and the KMnO₄-containing mixed acidic solution. As shown in **Figure S1b**, it is obvious that incorporation of KMnO₄ into the concentrated 1:2 (v:v) HNO₃:H₂SO₄ mixture significantly boosts capacitive performance of the carbon cloth. We also tailored the surface density of the functional groups by manipulating the time of exposure of the carbon cloth pieces with the KMnO₄ incorporated 1:2 (v:v) HNO₃:H₂SO₄ mixture. As presented in **Figure S1c**, and **Table S1**, treatment of the carbon cloth pieces for 60 min provides the best result. The redox peaks in the CV curves of the FCC electrode can be attributed to the redox reactions of the -C=O, -C-OH and -COOH functionalities:^{1,2}



Enrichment of the carbon cloth surface with diverse functional groups induces three main advantages: (i) improving the surface hydrophilicity; (ii) contributing to the pseudocapacitive charge storage *via* fast Faradaic redox reactions; and (iii) paving the way for efficient coating of carbon cloth with the polydopamine film.³

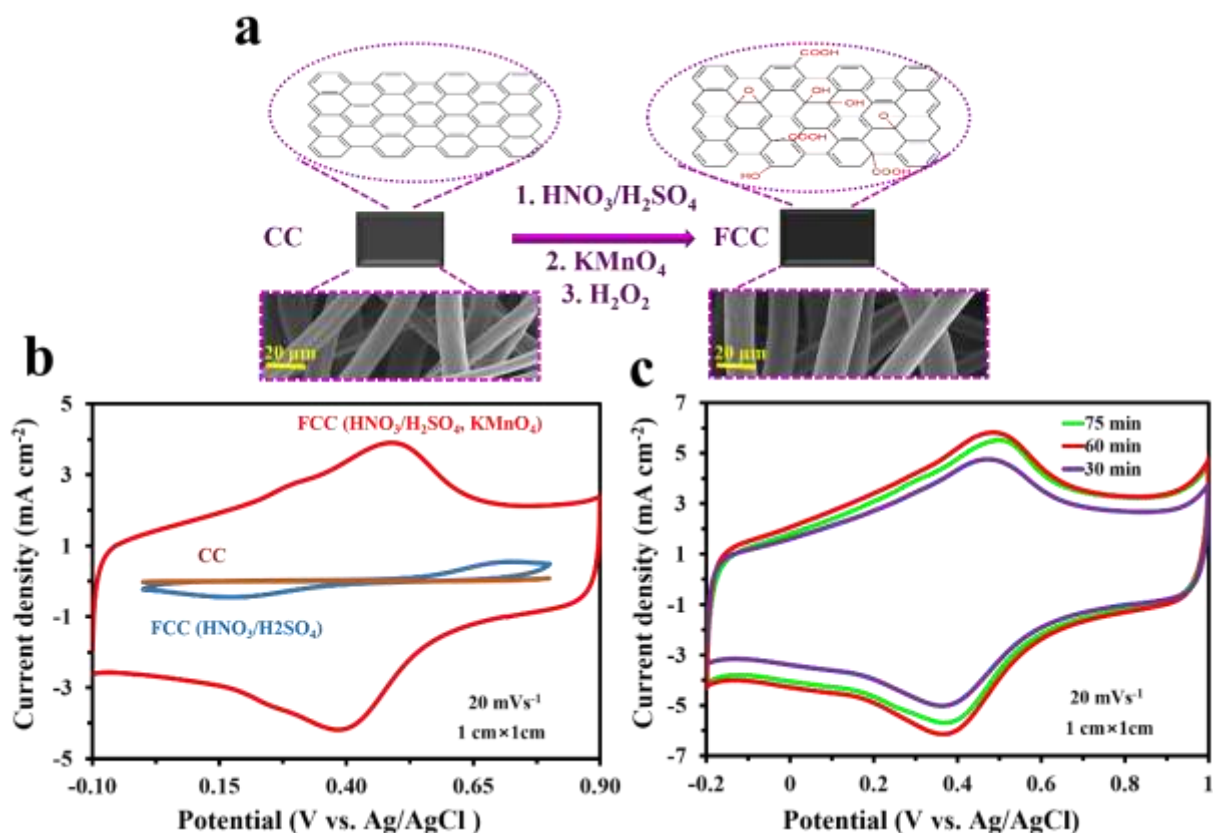


Figure S1. Functionalization of carbon cloth and its characterization. (a) Schematic illustration for the functionalization of carbon cloth *via* an acid treatment process. (b) CV curves of the pristine carbon cloth (CC) as well as the functionalized carbon cloth (FCC) prepared *via* treatment with a 1:3 (v:v) mixture of concentrated HNO₃:H₂SO₄ at 60 °C for 2 h and the one treated with the KMnO₄ incorporated 1:2 (v:v) HNO₃:H₂SO₄ mixture (scan rate = 20 mV s⁻¹ and the electrolyte is an aqueous 1.0 M H₂SO₄ solution). (c) CV curves of the FCC electrodes prepared *via* treatment with the KMnO₄ incorporated 1:2 (v:v) HNO₃:H₂SO₄ mixture for 30, 60, and 70 min at a scan rate of 20 mV s⁻¹ in an aqueous 1.0 M H₂SO₄ electrolyte.

Table S1. Energy Storage Performance of the FCC electrodes Presented in Figure S1c

Reaction time with KMnO₄	$\int I dV / (\text{mA V})$	Areal Capacitance (mF cm⁻²)
30 min	1.97	98.5
60 min	3.3	165.0
90 min	2.43	110.4

2. Synthesis of Polydopamine

2.1. Polydopamine Synthesis with a Constant Potential Method

We used CV, constant potential, and pulse potential methods for the preparation of the polydopamine film. The CV method did not provide suitable results. For electro-polymerization of dopamine by a double-potential step method, we applied the optimized nucleation pulse of 0.6 V vs. Ag/AgCl for a short time of 20 s. After that, the growth pulse of 0.5 V vs. Ag/AgCl was applied for 600.0 s. The synthesis solution contains 2.0 mg mL⁻¹ of dopamine hydrochloride in a typical phosphate buffer solution (PBS, 0.1 M, pH 7.4). After electrodeposition, the obtained PDA-FCC electrodes were washed with distilled water and dried at 60 °C for 3 h. The obtained PDA-FCC electrodes were activated in an aqueous 1.0 M H₂SO₄ electrolyte by applying 30 CV cycles at a sweep rate of 20 mV s⁻¹.

2.2. Polydopamine Synthesis *via* a Pulse Electrodeposition Method

This electro-deposition method allows for fine control over the particle size and morphology of the electro-synthesized PDA film. The potential of the working electrode is stepped from a rest potential to the optimized potential of 0.6 V for 0.5 s, where the nucleation takes place. After 0.5

s rest, the potential is stepped to 0.5 V for the optimized time of 0.5 s, a potential where no further nucleation can occur, instead the formed nuclei grow. GCD profiles of the PDA-FCC electrodes, prepared at different pulse-On times (t_{On}) are presented in **Figure S2** (the electrolyte is a 1.0 M H_2SO_4 solution). As can be seen, the $t_{\text{On}} = 0.5$ s provides the best performance (specific capacitance of 626 F g^{-1} at a discharge specific current of 1.0 A g^{-1}).

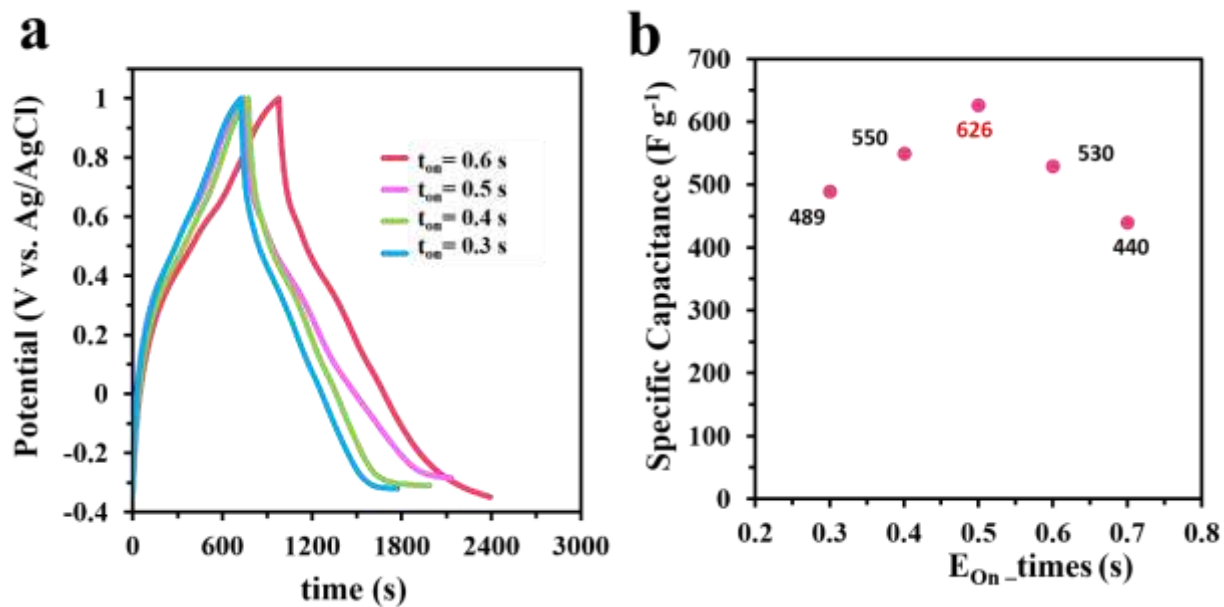


Figure S2. Optimization of the pulse deposition of polydopamine. (a) GCD profiles at a specific current of $1 A g^{-1}$ for the pulse deposited PDA-FCC electrodes. For preparation of this electrode, the potential is stepped from a rest potential to 0.6 V for 0.5 s for the first pulse, and then the potential is stepped to 0.5 V for the different times of 0.6, 0.5, 0.4 and 0.3 s; (b) The change in specific capacitance as a function of the t_{on} for the pulse deposited PDA-FCC electrodes.

3. Characterization of the Samples

3.1. EDS Spectroscopy

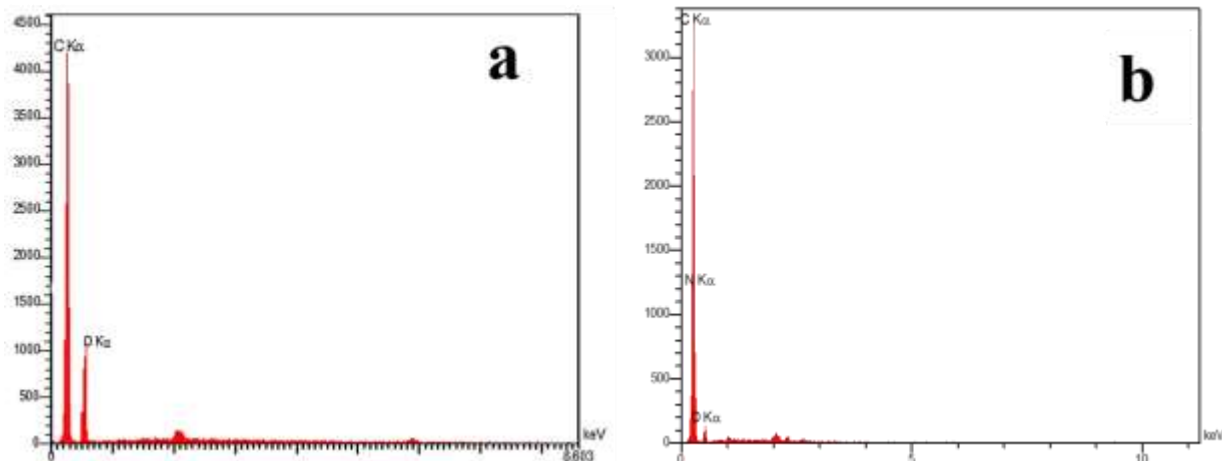


Figure S3. EDS spectra of the (a) FCC and (b) PDA-FCC electrodes, in which the peaks of N related to the presence of polydopamine in the PDA-FCC sample can be easily seen.

3.2. XPS Analysis

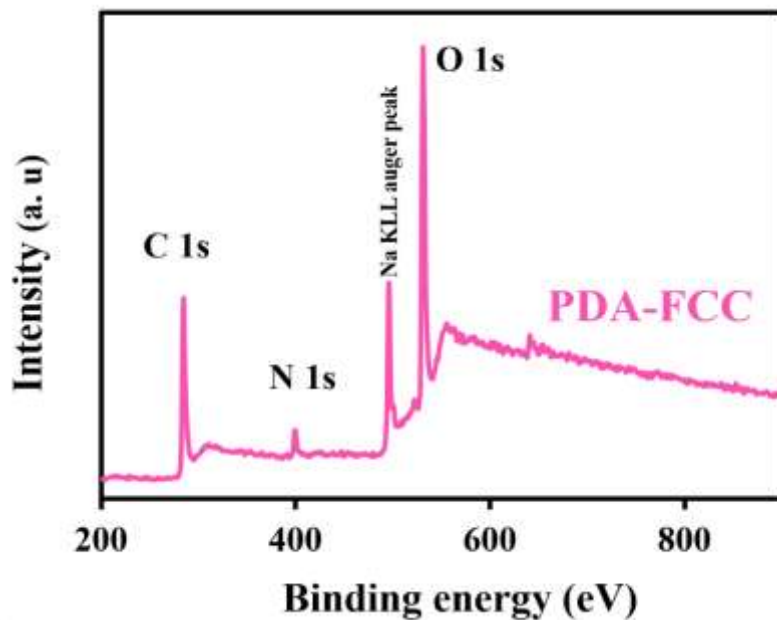


Figure S4. The survey XPS spectrum of the PDA-FCC.

Table S2. Contributions of Individual N-containing Moieties in the Core Level N 1s Spectra of the Pulse- and CP-deposited PDA-FCC Electrodes

Sample	Nitrogen content (%)			
	-N=	-NH-	-NH ₂	Total
PDA-FCC (Pulse)	0.8 (22.9 %)	2.1 (60%)	0.6 (17.1%)	3.5
PDA-FCC (CP)	1.2 (48%)	0.8 (32%)	0.5 (20%)	2.5

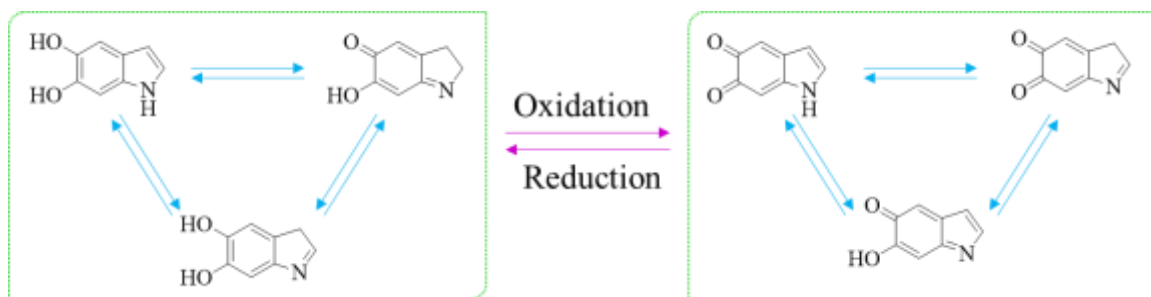


Figure S5. Tautomers of the possible intermediates formed in the oxidative polymerization of dopamine

3.3. XRD Analysis

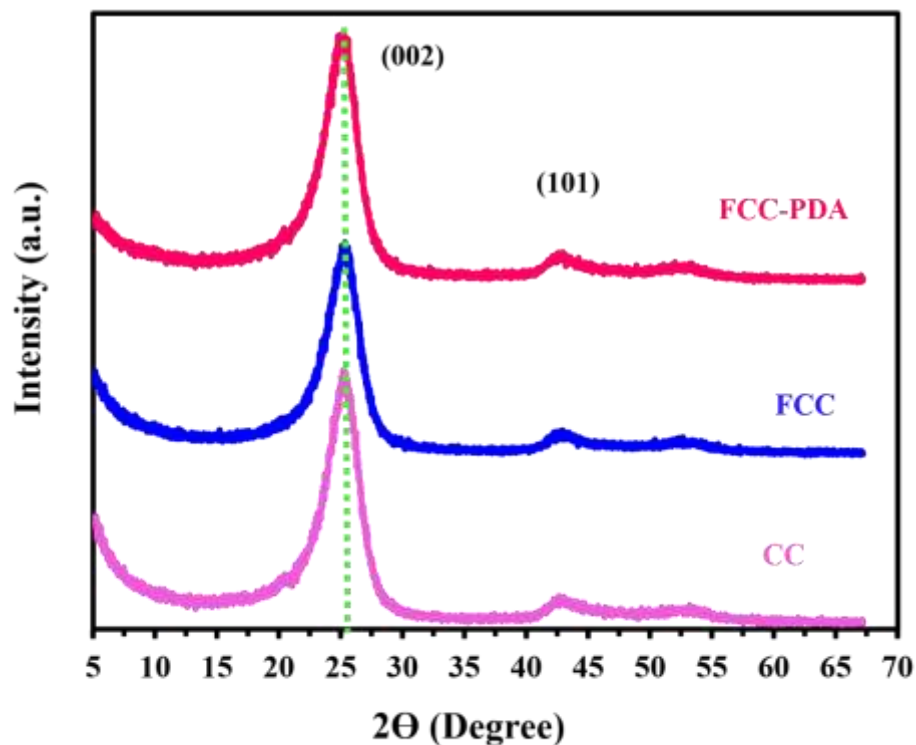


Figure S6. XRD patterns of the CC, FCC and PDA-FCC samples.

4. Wettability Studies

Wettability of the electrode active materials, which is determined by the type of the surface functionalities, is an important parameter that influences the capacitive performance of the materials. **Figure S6** shows photographs of the pristine CC as well as the FCC and PDA-FCC electrodes after a droplet of 1.0 M H_2SO_4 aqueous solution is placed on their surface. While the droplet remains on the hydrophobic pristine CC surface with an apparent contact angle of 103° , the droplets were completely absorbed into the hydrophilic FCC and PDA-FCC. After the acidic KMnO_4 treatment, the FCC surface is functionalized with oxygen-containing functional groups

that enormously improve the wettability of the FCC. The high nitrogen content of the PDA-FCC could also contribute positively to improve the wettability of the PDA-FCC electrode.

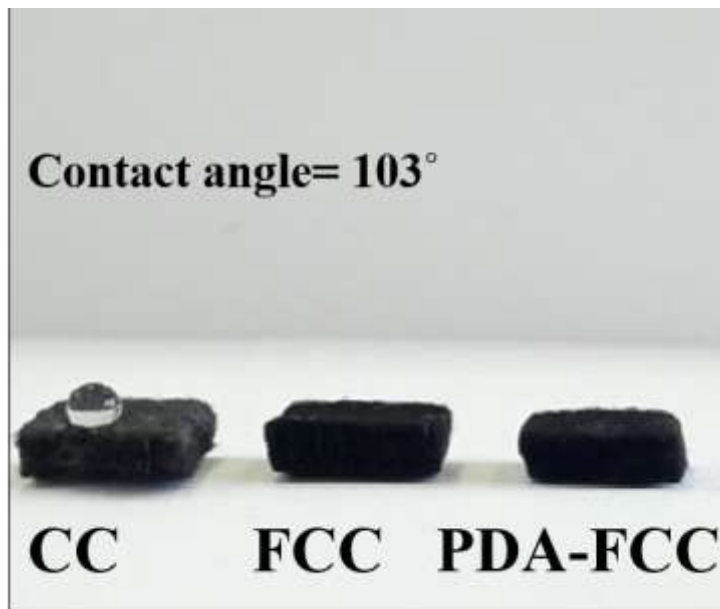


Figure S7. photographs of the pristine CC as well as the FCC and PDA-FCC electrodes after applying a drop of 1.0 M H₂SO₄ aqueous solution.

The electrolyte uptake of the PDA-FCC is significantly higher than that of the FCC (**Video S4**). The non-wetted surface area does not contribute to the capacitive energy storage, because an electrical double layer is formed only on the area wetted by the electrolyte. Functionalization of the pristine CC followed by electrodeposition of polydopamine facilitates the transport of the electrolyte ions into the inner pores of the electrode active materials, thus, improving the ionic conductivity, and making it easier for ions to form a double layer in the impregnated pores, which benefits the supercapacitive performance of the electrode.

5. Investigation of the Electrochemical Performance of the PDA-FCC Electrodes

5.1. CV curves of the Constant Potential Deposited PDA-FCC Electrode

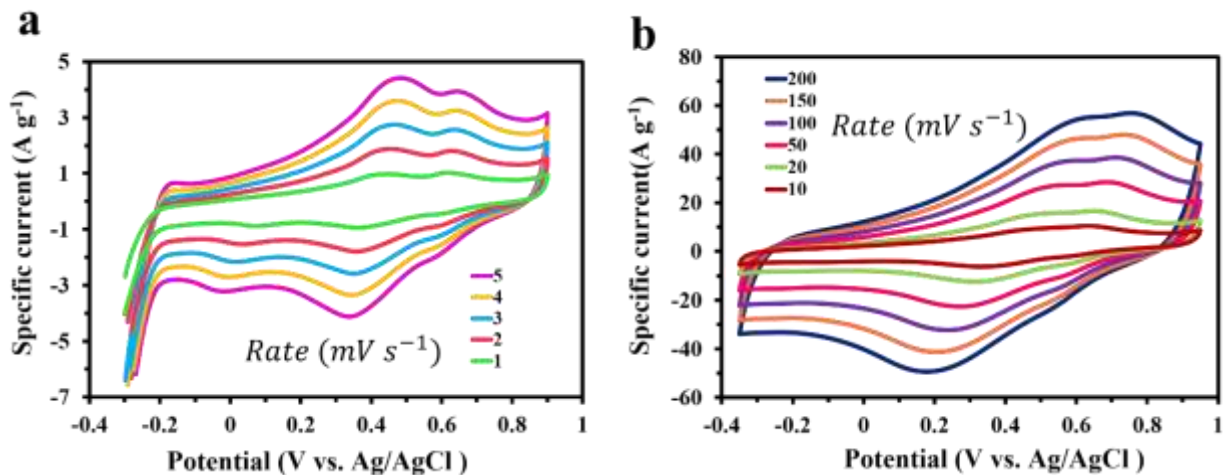


Figure S8. Scan rate study of the constant potential deposited PDA-FCC electrode. CV curves of the constant potential deposited PDA-FCC electrode at various scan rates in an aqueous 1.0 M H₂SO₄ electrolyte at different scan rates ranging from 1-200 mV s⁻¹.

5.2. CV Curves of the Pulse Deposited PDA-FCC Electrode

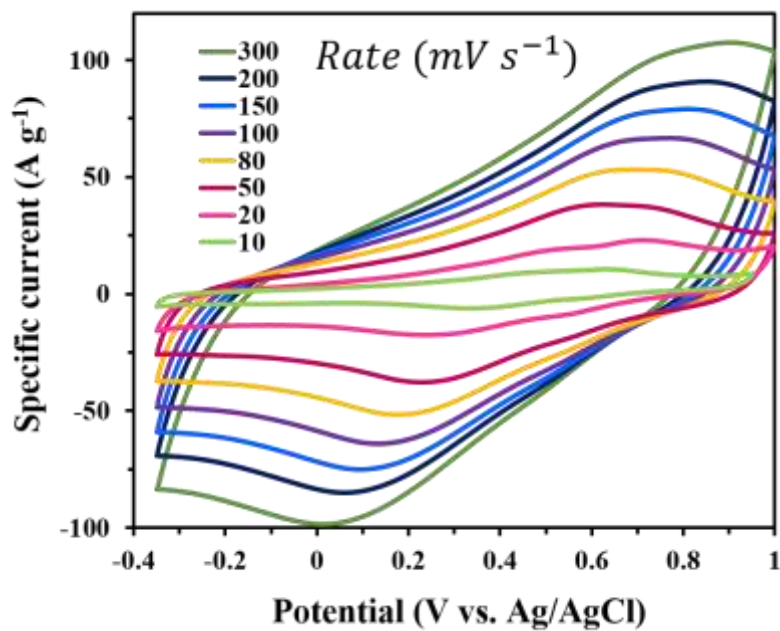


Figure S9. CV curves of the pulse potential deposited PDA-FCC electrode at various scan rates from 10 to 300 mV s⁻¹ in an aqueous 1.0 M H₂SO₄ electrolyte.

5.3. GCD Profiles of the Constant Potential Deposited PDA-FCC Electrode

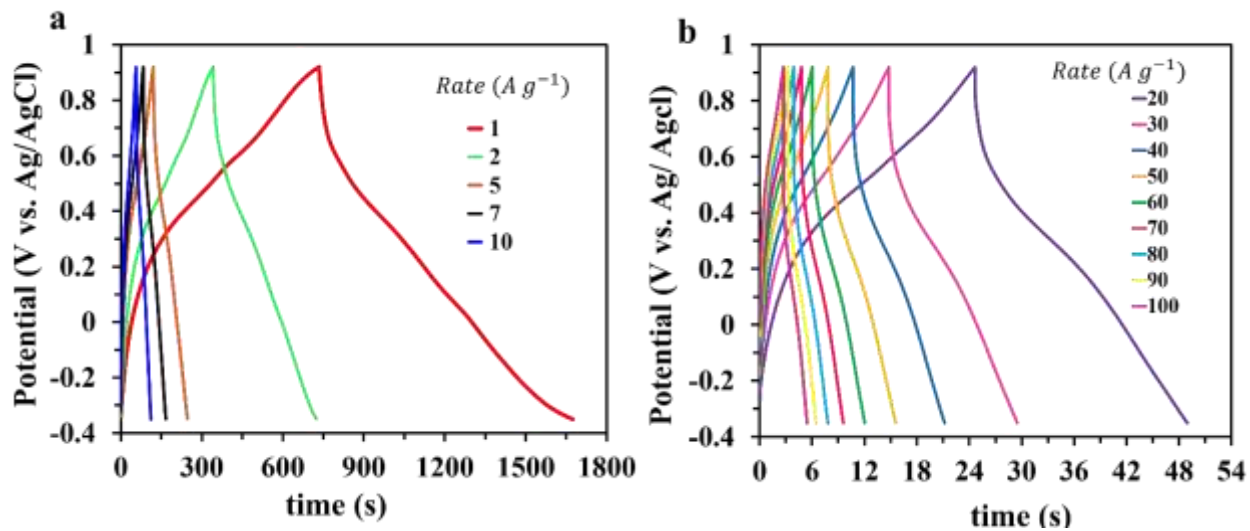


Figure S10. GCD profiles of the PDA-FCC electrode at different specific currents in an aqueous 1.0 M H_2SO_4 electrolyte: (a) 1-10 $A g^{-1}$ and (b) 20-100 $A g^{-1}$.

Table S3. Comparison of the Electrochemical Performance of the PDA-FCC Electrode with other Pseudocapacitive Materials.

Electrode material	Polymerization Method	Specific Capacitance at current density	Capacitive Retention (%) at current density	Electrolyte	Potential (V)	ref
Pt/graphene-PANI paper	Electropolymerization (constant potential)	763 F g ⁻¹ at 1 A g ⁻¹	64.2% at 10 A g ⁻¹	1.0 M H ₂ SO ₄	1.0	4
Stainless steel /nanosheets PPy	Electropolymerization (cyclic voltammetry)	584 F g ⁻¹ at 2 mVs ⁻¹	73.11% at 20 mA cm ⁻²	0.5 M H ₂ SO ₄	1.0	5
MnO ₂ nanoflakes @PPy Nanowires core/shell on activated carbon fiber cloth (ACFC /(MnO ₂ NFs@PPy NWs)	Chemical	276 F g ⁻¹ at 2 A g ⁻¹	72.5% at 20 A g ⁻¹	1.0 M Na ₂ SO ₄	0.9	6
carbonized polypyrrole (CPPy)-coated MnO ₂ micronodule (MnO ₂ @CPPy)	Chemical	9.84 F cm ⁻² at 10 mV s ⁻¹	91% at 200 mV s ⁻¹	1.0 M KOH	0.9	7
Functionalized carbon cloth-PPy (FCC/PPy)	Electropolymerization (constant Current)	341.2 9.84 F cm ⁻² at 1 mA cm ⁻²	70% at 20 mA cm ⁻²	5.0 M LiCl	0.8	8
PPy/Ti ₃ C ₂ T _x	Chemical	416 F g ⁻¹ at 5 mV s ⁻¹	62% at 100 mV s ⁻¹	1.0 M H ₂ SO ₄	0.55	9
GC/dopamine-mediated graphene hybrid – silver nanoparticles (GC/RGO-DA-Ag NP hybrid)	-	172.2 mF cm ⁻² at 10 mV s ⁻¹	-	5.0 mM K(CN) and 1.0 M KCl	0.8	10
Polydopamine-incorporated graphene oxide poly-(3,4-ethylenedioxythiophene) ITO/ PDA-GO-PEDOT	Chemical	126 F g ⁻¹ at 1 A g ⁻¹	73% at 10 A g ⁻¹	0.1 M LiClO ₄	1.0	11
Ni foam /Ni(HCO ₃) ²⁻ polydopaminereduced graphene oxide (Ni foam/Ni(HCO ₃) ²⁻ PDA-RGO)	Chemical	788 C g ⁻¹ at 1 A g ⁻¹	42% at 10 A g ⁻¹	4.0 M KOH	0.7	12
PDA /Ti ₃ C ₂ T _x	Chemical	715 mF cm ⁻² (260 F g ⁻¹) at 2 mV s ⁻¹ (1 A g ⁻¹)	52% at 100 mV s ⁻¹	1.0 M H ₂ SO ₄	0.55	13
Polypyrrole (PPy) hollow nanotubes (PNTs)	Chemical	240 F g ⁻¹ at 1 A g ⁻¹	31% at 6 A g ⁻¹	0.5 M HCL	0.5	14
		270 F g ⁻¹ at 1 A g ⁻¹	27% at 6 A g ⁻¹	0.5 M HCl + dopamine		
		724 F g ⁻¹ at 1 A g ⁻¹	69% at 6 A g ⁻¹	Polydopamine		
Polydopamine-coated Functionalized Carbon Cloth (PDA-FCC)	Electropolymerization (constant potential)	546 F g ⁻¹ (277 F g ⁻¹ total mass) at 1 A g ⁻¹	43% at 50 A g ⁻¹	1.0 M H ₂ SO ₄	1.3	This work
	Electropolymerization (Pulse)	626 F g ⁻¹ (363 F g ⁻¹ total mass) at 1 A g ⁻¹	47% at 50 A g ⁻¹			

5.4. EIS Characterization of the PDA-FCC Electrode

Table S4. The Values of Equivalent Circuit Parameters for the PDA-FCC Electrode at various potentials presented in Figure 4e.

Applied potential	ESR (Ω)	R_1 (Ω)	CPE_1 ($F s^{n-1}$)	n_1	$R_2(\Omega)$	CPE_2 ($F s^{n-1}$)	n_2	W ($\Omega s^{-1/2}$)	CPE_3 ($F s^{n-1}$)	n_3
0.3 V	0.87	1.73	0.63	0.18	1.2	0.01	0.63	0.28	0.22	0.85
0.4 V	0.75	1.39	0.02	0.38	1.53	2.9	0.88	0.12	0.43	0.84
0.5 V	0.84	1.26	0.01	0.47	0.03	0.16	0.45	0.79	0.22	0.74
0.6 V	0.85	1.11	6×10^{-3}	0.51	0.01	1.8	0.75	0.15	0.21	0.80
0.7 V	0.86	1.05	3×10^{-3}	0.59	1.28	1.12	0.82	1.61	0.19	0.82
OCP	0.94	0.43	5×10^{-3}	0.80	0.65	0.01	0.80	0.45	0.22	0.80

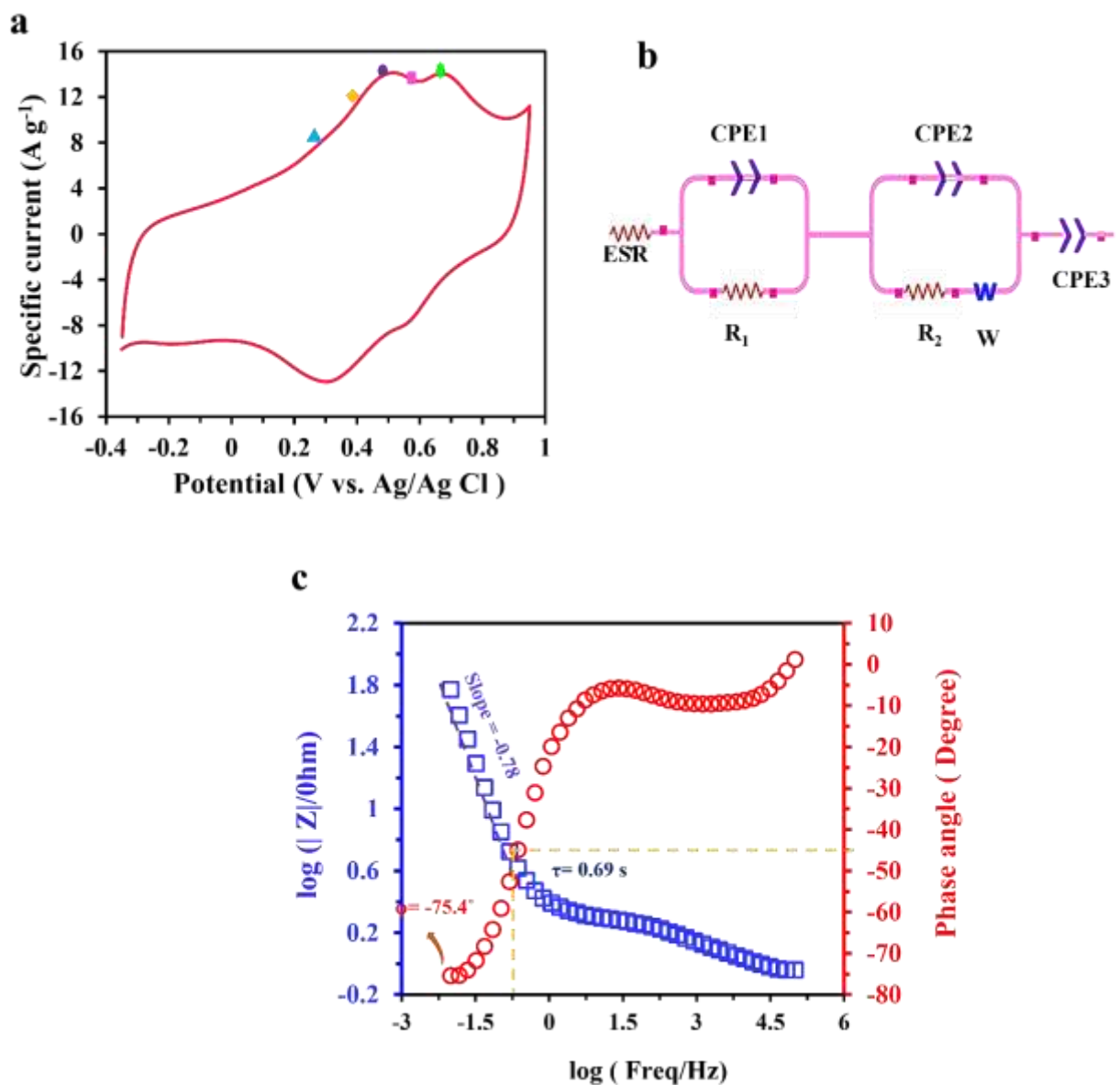


Figure S11. EIS characteristics of the PDA-FCC electrode in an aqueous 1.0 M H₂SO₄ electrolyte. (a) CV of the PDA-FCC electrode in which the potentials of 0.3, 0.4, 0.5, 0.6, and 0.7 V are marked. (b) A magnified high frequency region at applied potential of 0.4 V vs. an Ag/AgCl reference electrode. (points refer to the real EIS data and the lines refer to the fits to the experimental data). (c) The proposed equivalent circuit used to fit the experimental EIS data (d) Bode plots (plot of total impedance and phase angle vs. log frequency) for the PDA-FCC electrode.

6. Deconvolution of the Contribution from Capacitive and Battery-like Processes

A crucial issue in the study of hybrid materials is the deconvolution of the contribution from capacitive and battery-like processes in the charge storage of the system. Supercapacitive charge storage mechanisms are divided into (i) capacitive non-Faradaic charge storage (referred to as electrochemical double layer capacitance, EDLC), and (ii) capacitive Faradaic charge storage (denoted as pseudocapacitance).^{15, 16} However, battery-like charge storage also involves Faradaic redox reactions, thus, not all Faradaic redox reactions contribute to pseudocapacitive charge storage. The kinetics of the capacitive Faradaic and battery-type Faradaic charge storage processes are completely different. In a capacitive Faradaic system, the current changes linearly with the sweep rate, whereas in a battery-type Faradaic process the current is proportional to the square root of the sweep rate. Thus, the relationship between the current and potential sweep rate can be generally expressed as.^{17, 18}

$$i(\nu) = a\nu^b \quad (\text{S3})$$

where i is the current (A), ν is the potential sweep rate (V s^{-1}), and a and b are arbitrary coefficients. as shows in **Figure S11**, the b -value can be obtained from the slope of the plot of $\log i$ versus $\log \nu$, with rearrangement of Equation S3 as:

$$\log i(\nu) = \log a + b \log(\nu) \quad (\text{S4})$$

A b -value of 0.5 indicates battery-type diffusion-controlled electrode processes, and a b -value of 1 indicates surface-controlled fast Faradaic redox processes (i.e. capacitive charge transfer process). Hybrid systems exhibit a b -value in between. The calculated b -value is 0.72, indicating both capacitor-like and battery-like charge storage processes are involved in the PDA-FCC electrode.

The contribution from capacitive and battery-like charge storage processes can be quantitatively calculated from the following general relationship:

$$i(V) = k_1 v + k_2 v^{1/2} \quad (\text{S5})$$

Equation (S5) can be rearranged as:

$$i(V)/v^{1/2} = k_1 v^{1/2} + k_2 \quad (\text{S6})$$

where, $i(V)$ is the measured current as a function of potential and k_1 and k_2 coefficients are related to the current contributions from capacitive and non-capacitive processes, respectively. Note that the maximum contribution from the battery-like processes is obtained at slow sweep rates. Thus, this analysis was conducted at slow sweep rates in the range from 1 to 5 mV s^{-1} . **Figure 3f** shows that the ratio of the capacitive charge storage (the shaded region) to the total charge is 73% at a sweep rate of 3 mV s^{-1} . The high-rate capability is enabled by a high capacitive contribution and also fast redox reaction kinetics in the PDA-FCC electrode.

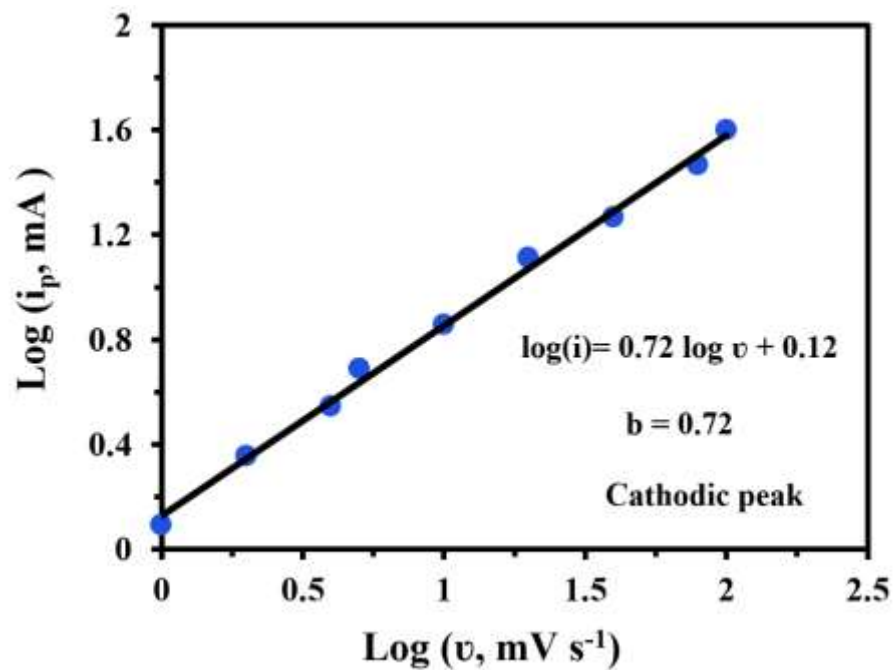


Figure S12. The $\log(i)$ versus $\log(v)$ plot of the cathodic peak currents (corresponding to the CVs presented in the main text, **Fig. 3b,c**).

7. Electrochemical characteristics of the symmetric PDA-FCC||PDA-FCC and FCC||FCC devices

7.1. CV Curves of the PDA-FCC||PDA-FCC Device

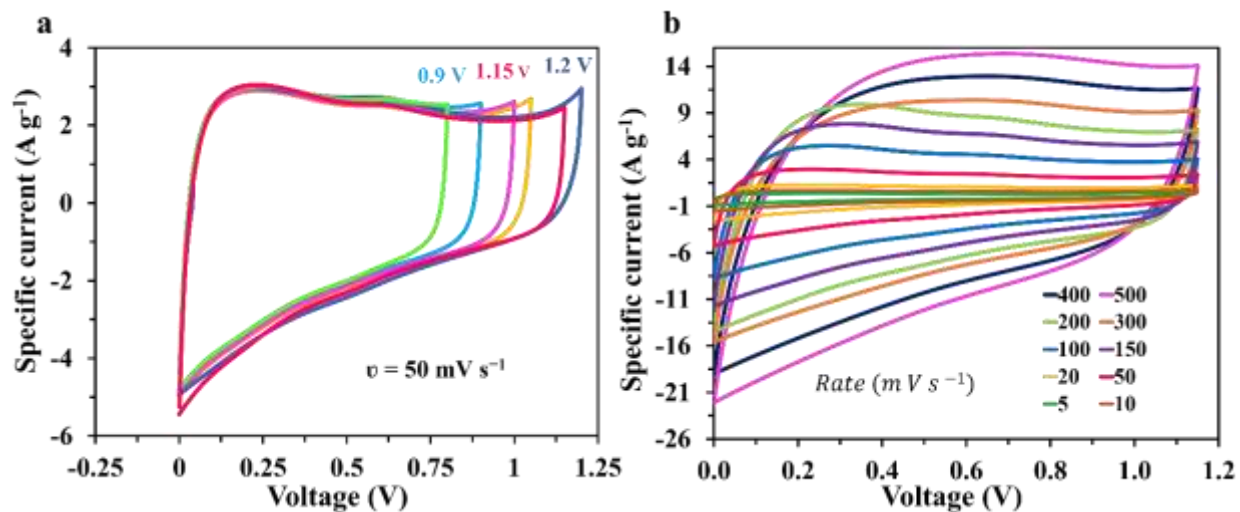


Figure S13. (a) CV curves of constant potential deposited PDA-FCC||PDA-FCC device at different voltage windows ($v = 50 \text{ mV s}^{-1}$). (b) CV curves of the constant potential deposited PDA-FCC||PDA-FCC device at various scan rates from 5 to 500 mV s^{-1} .

7.2. CV Curves of the FCC||FCC Device

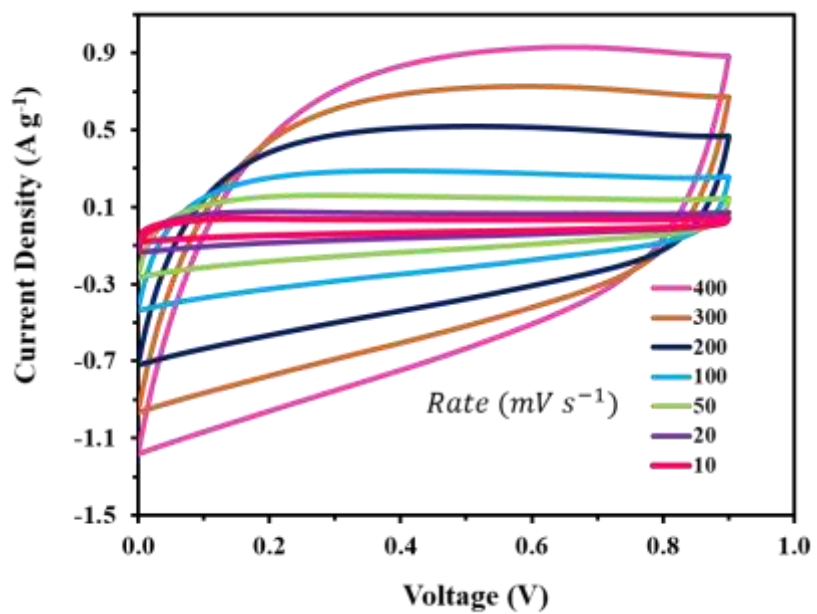


Figure S14. CV curves of the FCC||FCC device at various scan rates from 10 to 400 mV s^{-1} .

7.3. Gravimetric, Volumetric and Areal Capacitances of the Constant Potential Prepared PDA-FCC||PDA-FCC Device

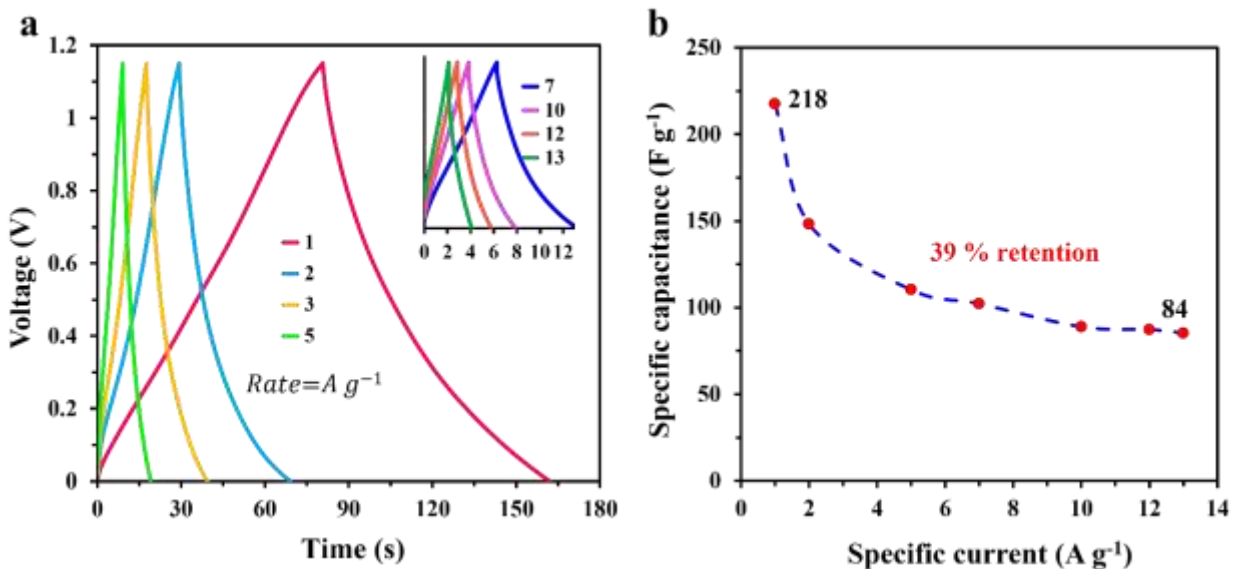


Figure S15. Gravimetric (Specific) capacitance. (a) GCD profiles of the solid-state symmetric PDA-FCC||PDA-FCC device in a PVA-in-H₂SO₄ gel electrolyte at various specific currents from 1 to 13 A g⁻¹. The Coulombic efficiency is nearly 100% in every cycle. (b) Rate capability study of the PDA-FCC||PDA-FCC device based on the gravimetric performance.

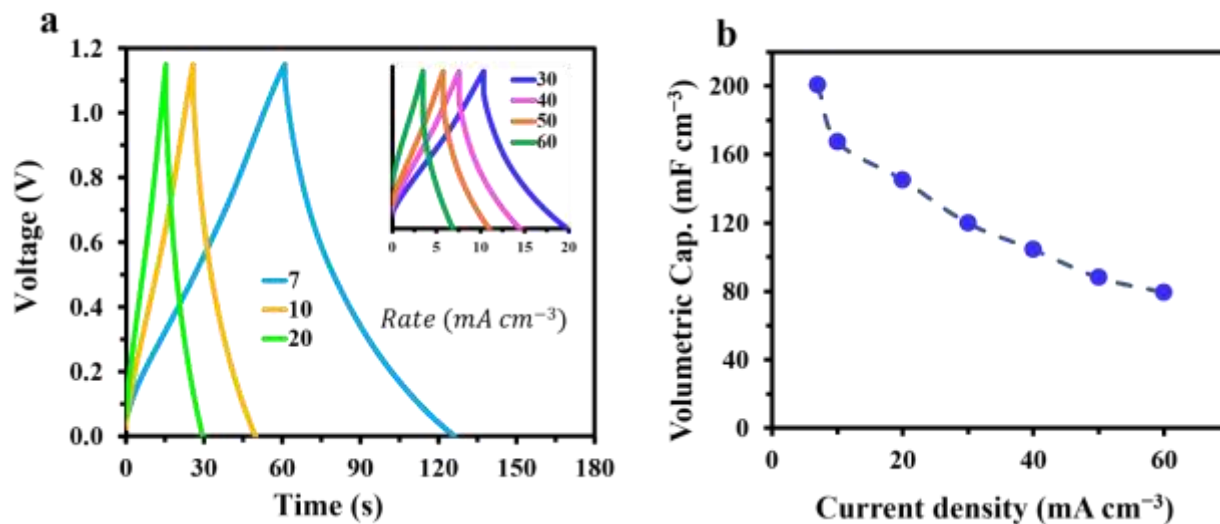


Figure S16. Volumetric capacitance. (a) GCD profiles of the solid-state symmetric PDA-FCC||PDA-FCC device in a PVA-in-H₂SO₄ gel electrolyte at various current densities from 5 to 70 mA cm⁻³. The Coulombic efficiency is nearly 100% in every cycle. (b) Rate capability study of the PDA-FCC||PDA-FCC device based on the volumetric performance.

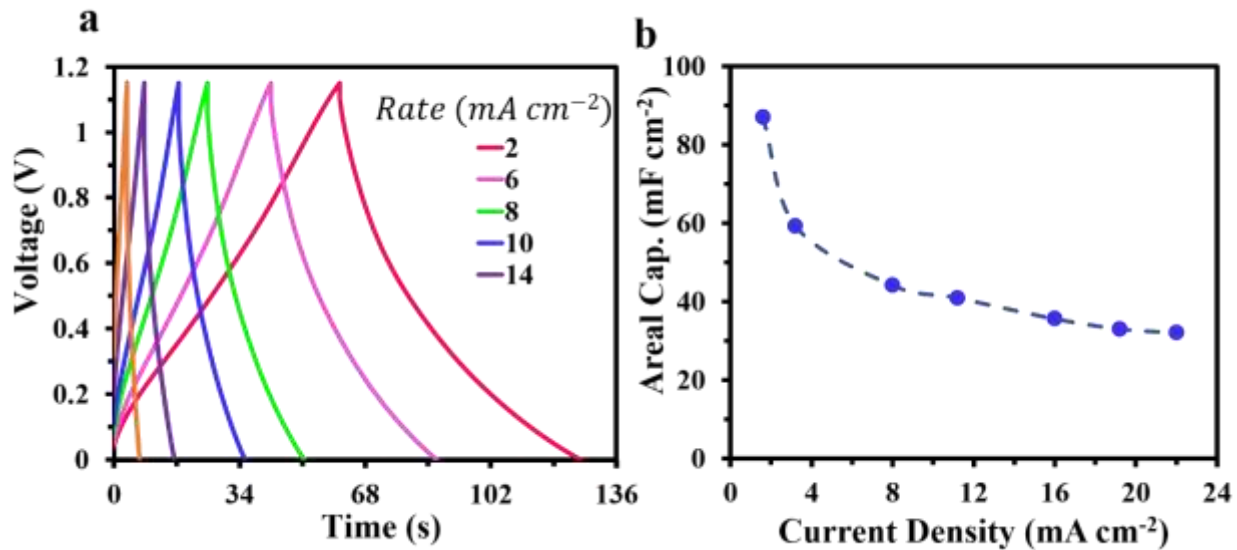


Figure S17. Areal capacitance. (a) GCD profiles of the solid-state symmetric PDA-FCC||PDA-FCC device in a PVA-in-H₂SO₄ gel electrolyte at various current densities from 2 to 25 mA cm⁻². The Coulombic efficiency is nearly 100% in every cycle. (b) Rate capability study of the PDA-FCC||PDA-FCC device based on the areal performance.

7.4. Cycling Stability Study

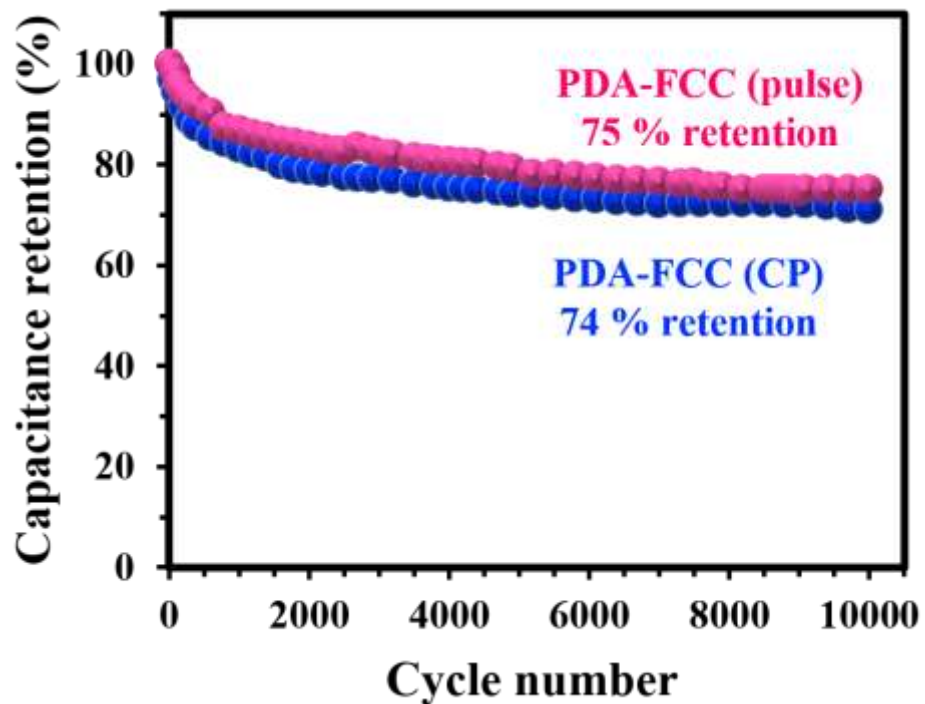


Figure S18. Evaluation of the Cycling Stability. Long term cycling stability of the constant potential (blue) and pulse potential (pink) prepared PDA-FCC||PDA-FCC devices over 10,000 GCD cycles at a specific current of 5 A g^{-1} in an aqueous $1.0 \text{ M H}_2\text{SO}_4$ electrolyte.

7. 5. EIS Studies

Figure S18 shows Nyquist plot and Bode plots of the PDA-FCC||PDA-FCC device in the frequency range from 100 kHz to 10 mHz. The Bode phase plot shows that the phase angle of the symmetric PDA-FCC||PDA-FCC device at low frequencies is -79.6° that is slightly less than the 90° observed for ideal capacitors. The slope of the Bode magnitude plot in the low frequency region is -0.75 . The deviation of the slope from -1 that is observed in ideal capacitors indicates that both capacitive and battery-like processes are involved in the energy storage system. The RC time constant, obtained from the Bode plot at phase angle of around -45° (-45.8°), is 0.31 s, demonstrating a much faster response time than many other conventional carbon-based electrochemical capacitors. Such a rapid frequency response can be attributed to the appropriate structure of the PDA-FCC electrode material that enhances the ion transport rate.

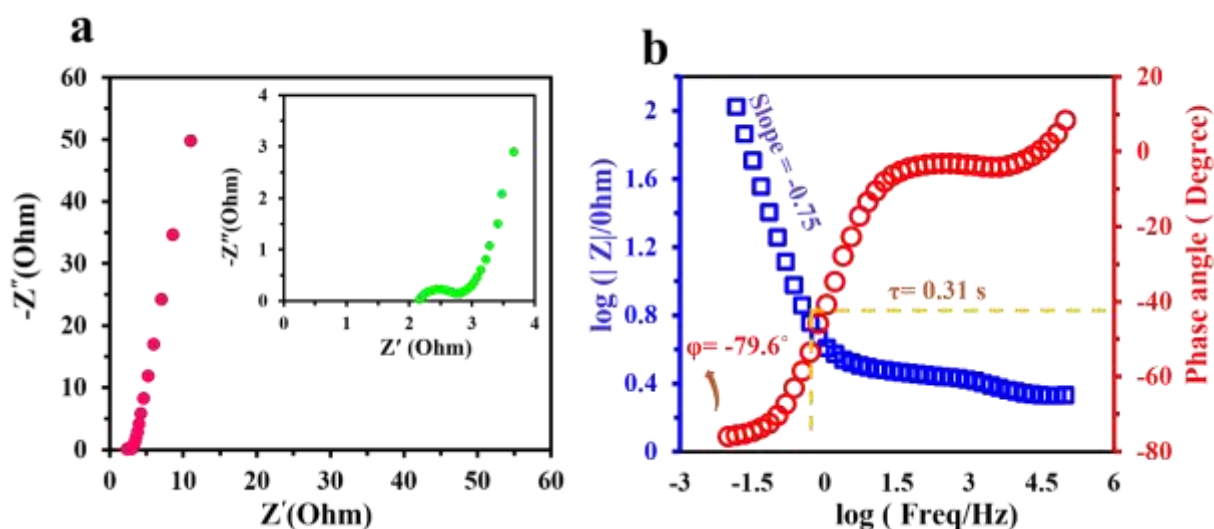


Figure S19. (a) Nyquist plot, and (b) Bode phase and magnitude plots of the solid-state symmetric PDA-FCC||PDA-FCC device over a frequency range from 100 kHz to 10 mHz. The inset of panel *a* shows the enlarged high-frequency region.

Table S5. Comparison of the Supercapacitive Performance of the Solid State PDA-FCC||PDA-FCC Device with Other Carbon- and Polymers-Based Symmetric Devices.

Symmetric device	Specific Capacitance at Current Density	Specific Energy	Cycles	Retention	Electrolyte	ΔV (V)	Ref
Poly(p-phenylenediamine)/graphene (PpPD/graphene)	84 F g ⁻¹ at 2 A g ⁻¹	8.6 Wh kg ⁻¹ at 500 W kg ⁻¹	1000	72 % at 10 A g ⁻¹	1.0 M H ₂ SO ₄	1.0	19
p-Phenylenediamine functionalized rGO(GHPPD)	303.88 F g ⁻¹ at 0.5 A g ⁻¹	20.53 Wh kg ⁻¹ at 1063.92 W kg ⁻¹	4000	86.15 % at 2 A g ⁻¹	2.0 M H ₂ SO ₄	0.8	20
Lignin-poly(3,4 ethylenedioxythiophene) Lignin/PEDOT	44 F g ⁻¹ at 0.1 A g ⁻¹	-	1000	52.2 % at 5 mV s ⁻¹	0.1 M HClO ₄	1.0	21
Highly conductive thick poly(3,4ethylene dioxythiophene):polystyrene sulfonate (HCTPEDOT:PSS)	50.1 F cm ⁻³ at 0.1 A cm ⁻³	3.15 mW h cm ⁻³ at 16160 mW cm ⁻³	8000	80 % at 100 mV s ⁻¹	PVA/H ₃ PO ₄ gel	1.0	22
ppy-layered Ti ₃ C ₂ ppy/l-Ti ₃ C ₂	35 mF cm ⁻² (2.39Fcm ⁻³) at 0.3 mA cm ⁻²	10 mW h cm ⁻³ at 500 mW cm ⁻³	10000	Almost 100% at 0.5 mA cm ⁻²	PVA-H ₂ SO ₄ gel	0.5	23
Acid-etched carbon cloth (AECC)	5310 mF cm ⁻² at 5 mA cm ⁻²	0.27 mW h cm ⁻³ at 1.32 W cm ⁻³	5000	93 % at 50 mA cm ⁻²	PVA-H ₂ SO ₄ gel	1.5	1
Carbon fibre cloths/ poly (3,4-ethylenedioxythiophene) CFC/PEDOT	203 F g ⁻¹ at 5 mV s ⁻¹	4.4 Wh kg ⁻¹ at 4250 W kg ⁻¹	12000	Almost 86% at 10 A g ⁻¹	1 M H ₂ SO ₄	0.8	24
Polyaniline-functionalized carbon cloth (PANI-FCC)	484 F g ⁻¹ at 1.0 A g ⁻¹	43 Wh kg ⁻¹	5000	87% at 1, 2, 5, 10, and 20 Ag ¹ (1000 cycle for each current density)	1 M H ₂ SO ₄	0.8	25
Self-doped polyaniline -functionalized carbon cloth (SPAN-FC)	67 F g ⁻¹ at 1.0 A g ⁻¹	7.8 Wh kg ⁻¹ 1 000 W kg ⁻¹	1000	95 % at 2 A g ⁻¹	0.5 M Na ₂ SO ₄	1.0	26
FCC-PANI array-rGO	197 mF cm ⁻² at 0.1 mA cm ⁻²	0.22 mW h cm ⁻³ 0.50 mW cm ⁻³	7000	91.3% at 5 mA cm ⁻²	PVA-H ₂ SO ₄ gel	0.8	27
Polypyrrole-polyoxometalate /reduced graphene oxide (PPy-PMo ₁₂ /rGO)	2.61 mF at 50 mA m ⁻²	-	1200	60 % at 200 mA m ⁻²	0.5 M H ₂ SO ₄	0.8	28
Polydopamine (PDA) modified reduced graphene oxide (rGO)/amino functionalized carbon nanotube rGO/CNTNH ₂ /PDA (GCP)	42.5 F g ⁻¹ at 0.5 A g ⁻¹	4.22 Wh kg ⁻¹ at 144 W kg ⁻¹	10000	98.9 % at 2 A g ⁻¹	6.0 M KOH	0.8	29
Activated carbon –polydopamine phosphomolybdic acid C-PDA/PMA-1 : 1	101 F g ⁻¹ at 1.0 A g ⁻¹	3.5 W h kg ⁻¹ 500 W kg ⁻¹	10000	108% at 2 A g ⁻¹	1.0 M H ₂ SO ₄	1.0	30
Activated carbon –polydopamine (C-PDA-1-3)	218 F g ⁻¹ at 1.0 A g ⁻¹	7.59 W h kg ⁻¹ 500 W kg ⁻¹	-	-	1.0 M H ₂ SO ₄	1.0	31
CP-deposited PDA-FCC PDA-FCC	54 F g ⁻¹ at 1.0 A g ⁻¹ (21 F g ⁻¹ total mass at 0.5 A g ⁻¹)	9.47 Wh kg ⁻¹ at 421 W kg ⁻¹ (3.7 Wh kg ⁻¹ total mass at 4430 W kg ⁻¹)	10000	74 % at 5 A g ⁻¹	PVA-H ₂ SO ₄ gel	1.15	This work
	174 mF cm ⁻² at 1.6 mA cm ⁻²						
	290 mF cm ⁻³ at 5 mA cm ⁻³						
Pulse-deposited PDA-FCC PDA-FCC	61 F g ⁻¹ at 1.0 A g ⁻¹ (24 F g ⁻¹ total mass at 0.5 A g ⁻¹)	11.7 Wh kg ⁻¹ at 385 W kg ⁻¹ (4.7 Wh kg ⁻¹ total mass at 6468 W kg ⁻¹)	10000	75 % at 5 A g ⁻¹	PVA-H ₂ SO ₄ gel	1.2	This work
	194 mF cm ⁻² at 1.6 mA cm ⁻²						
	324 mF cm ⁻³ at 5 mA cm ⁻³						

8. Calculations

Areal capacitance of the FCC and PDA-FCC electrodes was calculated from the CV curve using the following equation:

$$C_a = \frac{\int IdV}{A \times v \times \Delta V} \quad (S7)$$

where C is the areal capacitance (mF cm^{-2}), $\int IdV$ is the integrated area under the backward scan of the CV curve (mA V), A is surface area of the electrode (cm^2), v is the potential scan rate (V s^{-1}), and ΔV is the potential window (V).

The gravimetric, volumetric and areal capacitance of the PDA-FCC electrode as well as the devices were calculated using the following equation based on the GCD profiles:

$$C = \frac{2I \int Vdt}{x \times \Delta V^2} \quad (S8)$$

where C (F g^{-1} , F cm^{-2} , or F cm^{-3}) is the capacitance, I represents the discharge current (A g^{-1} , A cm^{-2} , or A cm^{-3}), $\int Vdt$ is the area under the GCD curve during the discharge (V.s), ΔV is the potential window (V), and x indicates the total mass of the polydopamine film deposited onto the FCC (g) or the area/volume of the PDA-FCC electrode. For the device level calculation, x represents the mass of the two electrode active materials, or the geometric area of the device. Volume (cm^3) of the device is obtained based on the volume of the two electrodes, current collectors and solid electrolyte (1.0 cm width \times 1.0 cm length \times 0.3 mm thickness).

The specific capacitance of each of the positive and negative electrodes can be calculated from the capacitance of a symmetric device using the following equation.

$$C_{\text{sp, electrode}} (\text{F g}^{-1}) = 4 \times C_{\text{device}} (\text{F g}^{-1}) \quad (S9)$$

Specific energy, specific power and of the devices were calculated using the following equations:

$$\mathbf{E}_{\text{sp}} = \frac{1000 \times \mathbf{I} \times \int \mathbf{V} \, \mathbf{dt}}{3600 \times \mathbf{m}} \quad (\text{S10})$$

$$\mathbf{P}_{\text{sp}} = \frac{\mathbf{E}_{\text{sp,device}} \times 3600}{t} \quad (\text{S11})$$

where E_{sp} (Wh kg^{-1}), P_{sp} (W kg^{-1}), specific power and energy efficiency, respectively, m indicates the total mass of the materials loaded on both the positive and negative electrodes (g), t is the discharge time (s).

Volume (cm^{-3}) of the device is calculated based on the volume of the two electrodes, current collectors, electrolyte, and separator (1.0 cm width \times 1.0 cm length \times 0.3 mm thickness).

Volumetric energy density and power density were calculated using the following equations:

$$\mathbf{E} (\text{Wh L}^{-1}) = \frac{1000 \times \mathbf{I} \times \int \mathbf{V} \, \mathbf{dt}}{3600 \times \mathbf{m}} \quad (\text{S12})$$

$$\mathbf{P} (\text{W L}^{-1}) = \frac{\mathbf{E} (\text{Wh L}^{-1}) \times 3600}{\Delta t (\text{s})} \quad (\text{S13})$$

References

1. Z. Miao, Y. Huang, J. Xin, X. Su, Y. Sang, H. Liu and J.-J. Wang, *ACS Appl. Mater. Interfaces*, 2019, **11**, 18044-18050.
2. E. Frackowiak and F. Beguin, *Carbon*, 2001, **39**, 937-950.
3. Y. He, Y. Zhang, X. Li, Z. Lv, X. Wang, Z. Liu and X. Huang, *Electrochim. Acta*, 2018, **282**, 618-625.
4. H.-P. Cong, X.-C. Ren, P. Wang and S.-H. Yu, *Energy Environ. Sci.*, 2013, **6**, 1185-1191.
5. D. P. Dubal, S. H. Lee, J. G. Kim, W. B. Kim and C. D. Lokhande, *J. Mater. Chem.*, 2012, **22**, 3044-3052.
6. W. He, C. Wang, F. Zhuge, X. Deng, X. Xu and T. Zhai, *Nano Energy*, 2017, **35**, 242-250.
7. J. S. Lee, D. H. Shin and J. Jang, *Energy Environ. Sci.*, 2015, **8**, 3030-3039.
8. D.-Y. Feng, Y. Song, Z.-H. Huang, X.-X. Xu and X.-X. Liu, *J. Power Sources*, 2016, **324**, 788-797.
9. M. Boota, B. Anasori, C. Voigt, M. Q. Zhao, M. W. Barsoum and Y. Gogotsi, *Adv. Mater.*, 2016, **28**, 1517-1522.
10. D. Bae, J. H. Han and W. Lee, *Compos. B Eng.*, 2018, **134**, 141-150.
11. I. Cha, E. J. Lee, H. S. Park, J.-H. Kim, Y. H. Kim and C. Song, *Synth. Met.*, 2014, **195**, 162-166.
12. J. Tian, Y. Xue, M. Wang, Y. Pei, H. Zhang and J. Wang, *Electrochim. Acta*, 2019, **296**, 49-58.
13. H. Wang, L. Li, C. Zhu, S. Lin, J. Wen, Q. Jin and X. Zhang, *J. Alloys Compd.*, 2019, **778**, 858-865.
14. B.-S. Yin, S.-W. Zhang, K. Ke and Z.-B. Wang, *Chem. Eng. J.*, 2019, **375**, 122056.
15. A. Noori, M. F. El-Kady, M. S. Rahmanifar, R. B. Kaner and M. F. Mousavi, *Chem. Soc. Rev.*, 2019, **48**, 1272-1341.
16. T. Brousse, D. Bélanger and J. W. Long, *J. Electrochem. Soc.*, 2015, **162**, A5185-A5189.
17. J. Liu, J. Wang, C. Xu, H. Jiang, C. Li, L. Zhang, J. Lin and Z. X. Shen, *Adv. Sci.*, 2018, **5**, 1700322.
18. M. Forghani and S. W. Donne, *J. Electrochem. Soc.*, 2018, **165**, A664-A673.
19. S. Ramaprabhu, *J. Mater. Chem.*, 2012, **22**, 18775-18783.
20. X. Lu, L. Li, B. Song, K.-s. Moon, N. Hu, G. Liao, T. Shi and C. Wong, *Nano Energy*, 2015, **17**, 160-170.
21. A. M. Navarro-Suárez, N. Casado, J. Carretero-González, D. Mecerreyes and T. Rojo, *J. Mater. Chem. A*, 2017, **5**, 7137-7143.
22. Z. Li, G. Ma, R. Ge, F. Qin, X. Dong, W. Meng, T. Liu, J. Tong, F. Jiang and Y. Zhou, *Angew. Chem. Int. Ed.*, 2016, **55**, 979-982.
23. M. Zhu, Y. Huang, Q. Deng, J. Zhou, Z. Pei, Q. Xue, Y. Huang, Z. Wang, H. Li and Q. Huang, *Adv. Energy Mater.*, 2016, **6**, 1600969.
24. M. Rajesh, C. J. Raj, R. Manikandan, B. C. Kim, S. Y. Park and K. H. Yu, *Mater. Today Energy*, 2017, **6**, 96-104.
25. M. Hashemi, M. S. Rahmanifar, M. F. El-Kady, A. Noori, M. F. Mousavi and R. B. Kaner, *Nano energy*, 2018, **44**, 489-498.
26. L.-J. Bian, F. Luan, S.-S. Liu and X.-X. Liu, *Electrochim. Acta*, 2012, **64**, 17-22.
27. P. Du, Y. Dong, H. Kang, X. Yang, Q. Wang, J. Niu, S. Wang and P. Liu, *ACS Sustainable Chem. Eng.*, 2018, **6**, 14723-14733.
28. Y. Chen, M. Han, Y. Tang, J. Bao, S. Li, Y. Lan and Z. Dai, *Chem. Commun.*, 2015, **51**, 12377-12380.
29. R. Zeng, H. Deng, Y. Xiao, J. Huang, K. Yuan and Y. Chen, *Compos. Commun.*, 2018, **10**, 73-80.
30. X. Chen, Q. Z. Song, W. X. He, P. P. Liu, Y. H. Xiao and J. Y. Liang, *Dalton Transact.*, 2019, **48**, 17321-17330.

31. Z. J. Zhang, G. L. Deng, X. Huang, X. Wang, J. M. Xue and X. Y. Chen, *Electrochim. Acta*, 2020, **339**, 135940.